JOURNAL OF GEOPHYSICAL RESEARCH, VOL. 111, C09007, doi:10.1029/2005JC003183, 2006

Fate of rising methane bubbles in stratified waters: How much methane reaches the atmosphere?

D. F. McGinnis,[1] J. Greinert,[2] Y. Artemov,[3] S. E. Beaubien,[4] and A. Wüest[1]

Received 22 July 2005; revised 12 May 2006; accepted 22 May 2006; published 2 September 2006.

[1] There is growing concern about the transfer of methane originating from water bodies to the atmosphere. Methane from sediments can reach the atmosphere directly via bubbles or indirectly via vertical turbulent transport. This work quantifies methane gas bubble dissolution using a combination of bubble modeling and acoustic observations of rising bubbles to determine what fraction of the methane transported by bubbles will reach the atmosphere. The bubble model predicts the evolving bubble size, gas composition, and rise distance and is suitable for almost all aquatic environments. The model was validated using methane and argon bubble dissolution measurements obtained from the literature for deep, oxic, saline water with excellent results. Methane bubbles from within the hydrate stability zone (typically below ~500 m water depth in the ocean) are believed to form an outer hydrate rim. To explain the subsequent slow dissolution, a model calibration was performed using bubble dissolution data from the literature measured within the hydrate stability zone. The calibrated model explains the impressively tall flares (>1300 m) observed in the hydrate stability zone of the Black Sea. This study suggests that only a small amount of methane reaches the surface at active seep sites in the Black Sea, and this only from very shallow water areas (<100 m). Clearly, the Black Sea and the ocean are rather effective barriers against the transfer of bubble methane to the atmosphere, although substantial amounts of methane may reach the surface in shallow lakes and reservoirs.

Citation: McGinnis, D. F., J. Greinert, Y. Artemov, S. E. Beaubien, and A. Wüest (2006), Fate of rising methane bubbles in stratified waters: How much methane reaches the atmosphere?, *J. Geophys. Res.*, *111*, C09007, doi:10.1029/2005JC003183.

1. Introduction

[2] The doubling of methane concentrations from 850 ppb to ~1750 ppb over the last 150 years [*Cicerone and Oremland*, 1988] is alarming, as methane has 21 to 25 times the global warming potential as the same mass of carbon dioxide [*Intergovernmental Panel on Climate Change*, 1996; *Lelieveld et al.*, 1998; *St. Louis et al.*, 2000]. Currently, anthropogenic inputs (e.g., rice paddies, livestock and biomass combustion) contribute ~71% to the atmospheric concentration [*Reeburgh*, 1996], while natural sources (e.g., wetlands, lakes and termites) contribute the remaining 29%. While the natural contribution from the oceans is estimated to be only 2–4% of the global atmospheric methane budget [*Judd et al.*, 2002], estimates vary from 1% for freshwater bodies [*Whiticar*, 2000] to about 2–10% for lakes [*Bastviken et al.*, 2004], while reservoirs are thought to comprise up to 18% of the anthropogenic methane flux [*St. Louis et al.*, 2000]. There is growing concern that much higher atmospheric concentrations will result in the future if a substantial amount of the huge methane pools stored in ocean [*Milkov*, 2004] and lake/reservoir sediments is released [*Buffett*, 2000].

[3] Methane produced in sediments or anaerobic waters can reach the atmosphere or surface mixed layer through turbulent diffusion, rising bubbles and even advective transport through plant roots [*Adams*, 2005; *Bastviken et al.*, 2004; *Joyce and Jewell*, 2003]. While turbulent transport dominates in deep systems, the release of methane bubbles is the most important pathway in shallow waters, particularly in the littoral zone where they are most likely to reach the atmosphere [*Adams*, 2005; *Joyce and Jewell*, 2003]. Bubbles from the sediments are released into marine (Figure 1a) and lacustrine (Figure 1b) waters due to dissolved gas supersaturation, shear stress from bottom currents or pressure decrease during reservoir drawdown [*Joyce and Jewell*, 2003], as well as the dissociation of methane hydrates in the ocean and deep lakes [*De Batist et al.*, 2002; *Granin and Granina*, 2002; *MacDonald et al.*, 2003; *Pecher et al.*, 2001; *Suess et al.*, 1999, 2001; *Torres et al.*, 2002; *Trehu et al.*, 1999; *Tryon et al.*, 2002; *Van Rensbergen et al.*, 2002]. Owing to the rapid vertical transport of methane by bubble ebullition there is growing concern over the contribution of this mechanism to the global methane budget [*Leifer and Patro*, 2002]. For

[1]Surface Waters–Research and Management, Swiss Federal Institute of Aquatic Science and Technology, Kastanienbaum, Switzerland.
[2]Marine Geosystems, Leibniz-Institut für Meereswissenschaften IFM-GEOMAR, Kiel, Germany.
[3]Institute of Biology of the Southern Seas, Sevastopol, Ukraine.
[4]Department of Earth Sciences, University "La Sapienza," Rome, Italy.

0148-0227/06/2005JC003183$09.00

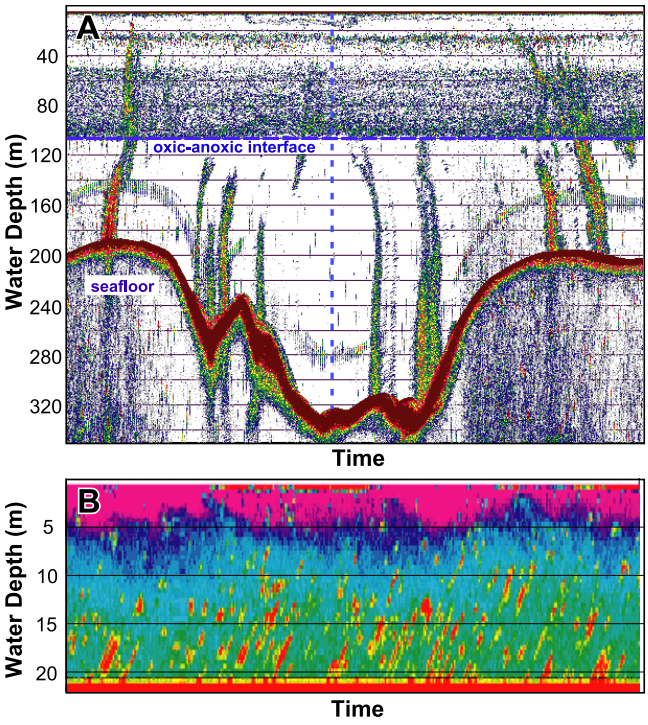

Figure 1. (a) Single-beam echogram showing the typical acoustic response of rising bubbles as a flare-like shape having high backscatter signals in the Black Sea [*Greinert et al.*, 2006]. The image shows several flares rising from different depths (x axis $\sim$ 22 min), with shallower flares almost reaching the sea surface after crossing the oxic/anoxic boundary at about 110 m. The strong signals in the oxic zone above 110 m water depth are caused by fish and zooplankton, whereas below this depth, the Black Sea provides ideal conditions for detailed acoustic studies of bubbles without other "disturbing" backscattering. The flares are tilted because of horizontal currents. The bending of the flares toward the middle of the image is caused by the turn of the ship on an opposing course (vertical dashed line). (b) Acoustic Doppler current profiler (ADCP) backscatter measurements from Iron Gate I dam on the Danube River (Romania). The strong backscatter data in the water column indicate bubbles released from the sediment in 21 m water depth (x axis $\sim$ 10 min) [*McGinnis et al.*, 2006].

example, methane bubble releases may increase in the future due to the construction of more reservoirs [*St. Louis et al.*, 2000] or the destabilization of hydrates due to global warming [*Buffett*, 2000].

[4] The importance of determining methane bubble transport and its possible impact on atmospheric concentrations becomes obvious when considering the large number of methane-bubbling seep sites reported worldwide using visual and acoustic investigations in both shallow and deep waters [*Dando et al.*, 1994; *Egorov et al.*, 2003; *Greinert et al.*, 2006; *Heeschen et al.*, 2003; *Hovland and Judd*, 1988; *Lewis and Marshall*, 1996; *MacDonald et al.*, 2005; *Naudts et al.*, 2006; *Paull et al.*, 1995; *Zimmermann et al.*, 1997]. These studies highlight the significance of in situ release conditions for controlling transfer processes. For example the depth and temperature of methane release has important implications, as bubbles formed within the hydrate stability zone (HSZ) ($\sim$400–500 m in lakes and oceans) dissolve much more slowly than those released above it [*Zhang*, 2003]. This reduced bubble dissolution rate was observed during experiments in Monterey Bay [*Rehder et al.*, 2002] and was further suggested by the observations of very high acoustic flares within the Guayamas Basin [*Merewether et al.*, 1985] and the Black Sea [*Greinert et al.*, 2006]. In this article, acoustic bubble observations are referred to as flares because of their flame-like appearance on the echogram (see Figure 1a). The extended bubble lifetime is likely due to the presence of a hydrate rim, which is believed to form rapidly around bubbles in the HSZ [*Maini and Bishnoi*, 1981] and inhibit mass transfer and alter bubble hydrodynamics [*Rehder et al.*, 2002]. Although the exact nature of the rim is not well understood, its existence is suggested from both laboratory [*Gumerov and Chahine*, 1998; *Maini and Bishnoi*, 1981] (see http://www.dynaflow-inc.com/Publication_DW/pdf_documents/web_hydrates.pdf) and field observations [*Rehder et al.*, 2002; *Topham*, 1984a]).

[5] The present study uses a simple bubble model to describe the vertical transport of methane through the water column after release from the sediments, with model results subsequently being compared to methane bubble data from the literature. The model is then used to attempt to explain the tall flares observed in the Black Sea and to address the questions, how much methane is transferred to the atmosphere via direct bubble transport, and what conditions inhibit or facilitate this transfer? We use the following approaches: (1) a single bubble model is developed using parameterizations that are applicable for a wide range of ambient water conditions in oceans and lakes; (2) the model is compared to data obtained by *Rehder et al.* [2002] from deep, saline waters above the HSZ and is calibrated to data obtained by *Rehder et al.* [2002] from within the HSZ; (3) the calibrated model is applied to explain extremely high flares observed in the Black Sea; and (4) finally, the model is used to estimate the potential amount of bubble-transported methane to reach the atmosphere from marine and lacustrine environments.

2. Study Sites, Data, and Methods

2.1. Data From Literature

[6] Literature data are primarily from *Rehder et al.* [2002], who measured the shrinkage of methane and argon bubbles released within and above the HSZ during remotely operated vehicle (ROV) experiments in Monterey Bay. Bubble release depths were obtained by personal communication with the author. Model boundary conditions for the Monterey Bay area consist of conductivity-temperature-depth (CTD) data from the National Oceanographic Data Center (NODC) at the NOAA web page (http://www.nodc.noaa.gov). The data are from a 1991 cruise with R/V *T. Washington*, taken within the WOCE project near Monterey Bay (35°47.4′N and 122°16.7′W (Figure 2)). Background methane concentrations were taken from unpublished data at the Hydrate Ridge site (44°26′N, 125°30′W), while dissolved argon and nitrogen concentrations were calculated according to *Weiss* [1970].

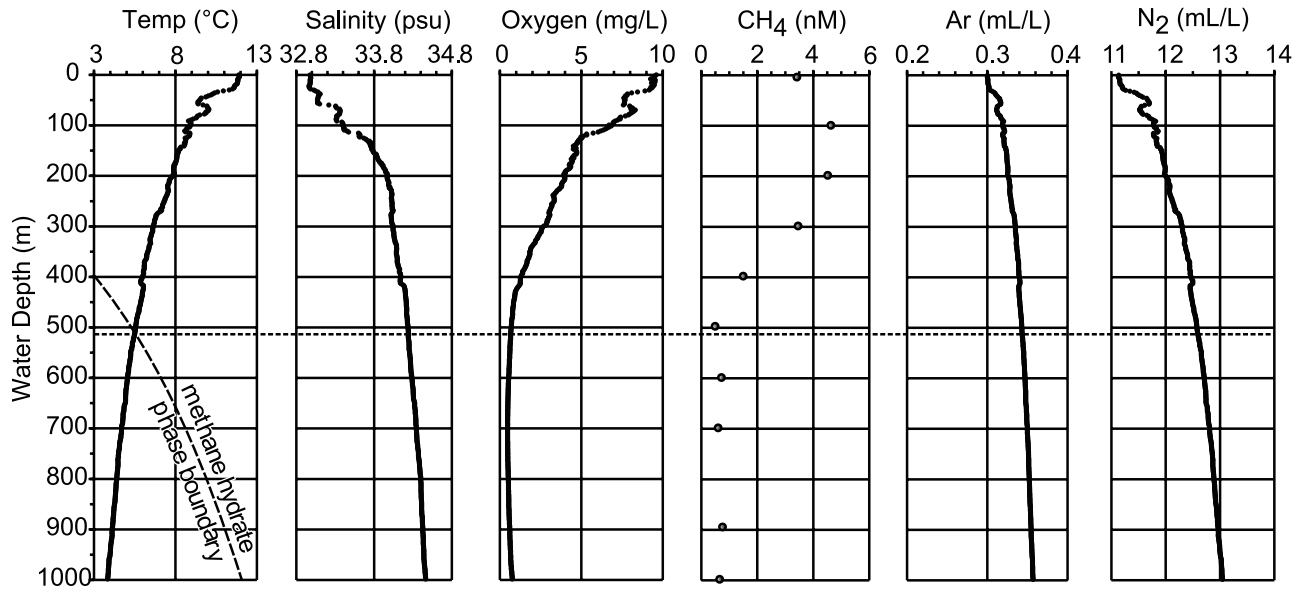

Figure 2. Physical and chemical parameters from Monterey Bay used to model bubble release experiments by *Rehder et al.* [2002]. The dashed horizontal line (~500 m depth) marks the phase boundary for pure methane hydrate at the in situ temperature and salinity conditions.

2.2. Black Sea

[7] A large data set of acoustic and geochemical measurements, together with direct bubble observations, exists from the EU-funded CRIMEA ("Contribution of high-intensity gas seeps in Black Sea to the methane emission to the atmosphere") project. More than 2000 bubble seeps west and southeast of the Crimea Peninsula were observed between 70 and 2090 m water depth [*Egorov et al.*, 2003; *Naudts et al.*, 2006]. This data set was collected from the Dnepr Paleo Delta area and the Sorokin Trough (Figure 3) during two cruises aboard R/V *Professor Vodyanitskiy* between May and June 2003 and 2004. Water column profiles were obtained by CTD casts and water sampling (Figure 4). Seep distributions, bubble sizes and rising speeds were determined by acoustic measurements, visual observations with towed systems and ROV deployments (Benthos MiniRover). During dives with the submersible JAGO (as part of the EU-funded project METROL), gas bubbles were collected directly at the seafloor with an inverted funnel to measure the initial gas composition (almost pure methane with −62 to −68 ^{13}C‰ PDB) and to determine the methane flux (0.55–1.44 mL/s at in situ pressure = 0.24–0.64 mmol/s).

[8] Water column measurements and water sampling were performed with a Sea-Bird SBE 911plus CTD (Sea-Bird Electronics, Inc., Washington, USA) equipped with a Beckman oxygen sensor and attached to a 12-bottle water sampling carrousel. The oxygen sensor data were calibrated via Winkler titration. Dissolved gases were measured directly on board using a vacuum degassing line [*Lammers and Suess*, 1994; *Rehder et al.*, 1999] and a Varian 3800 gas chromatograph (CH_4 to C_3H_8, Ar, N_2).

[9] Several CTD casts from the shelf, the slope and the open waters of the Black Sea were used to obtain the stratification and constituent concentrations for the different model runs. In general, the Black Sea water column is characterized by significant changes in temperature and oxygen concentrations linked to the oxic/anoxic interface (between ~110 and 125 m water depth (Figure 4)). Methane concentrations on the shelf increase rapidly with depth due to the large volumes of methane released from the organic rich shelf sediments. It is obvious in the Black Sea that methane bubbles are released in highly variable conditions (anoxic and oxic; above and within the HSZ; low to high salinity), emphasizing the importance of a widely applicable bubble model.

[10] Remote acoustic bubble observation is an ideal, noninvasive tool to study the behavior and fate of bubbles in the water column [*Greinert et al.*, 2006; *Ostrovsky*, 2003]. In this work, the methods described by *Artemov* [2006] were used for acoustic bubble seep detection, digital data processing and flare height determination, as well as calculation of the size, shrinkage rate and rising speed of individual bubbles. A single-bubble tracking technique was applied to obtain data for rising speeds and shrinkage

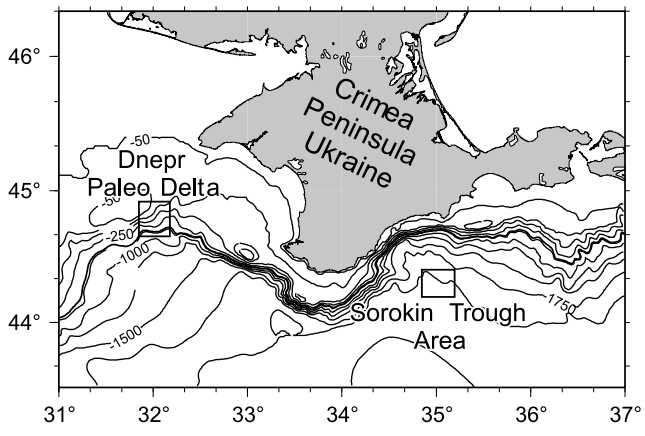

Figure 3. Location of the two study areas in the Black Sea: the Dnepr Paleo Delta and Sorokin Trough.

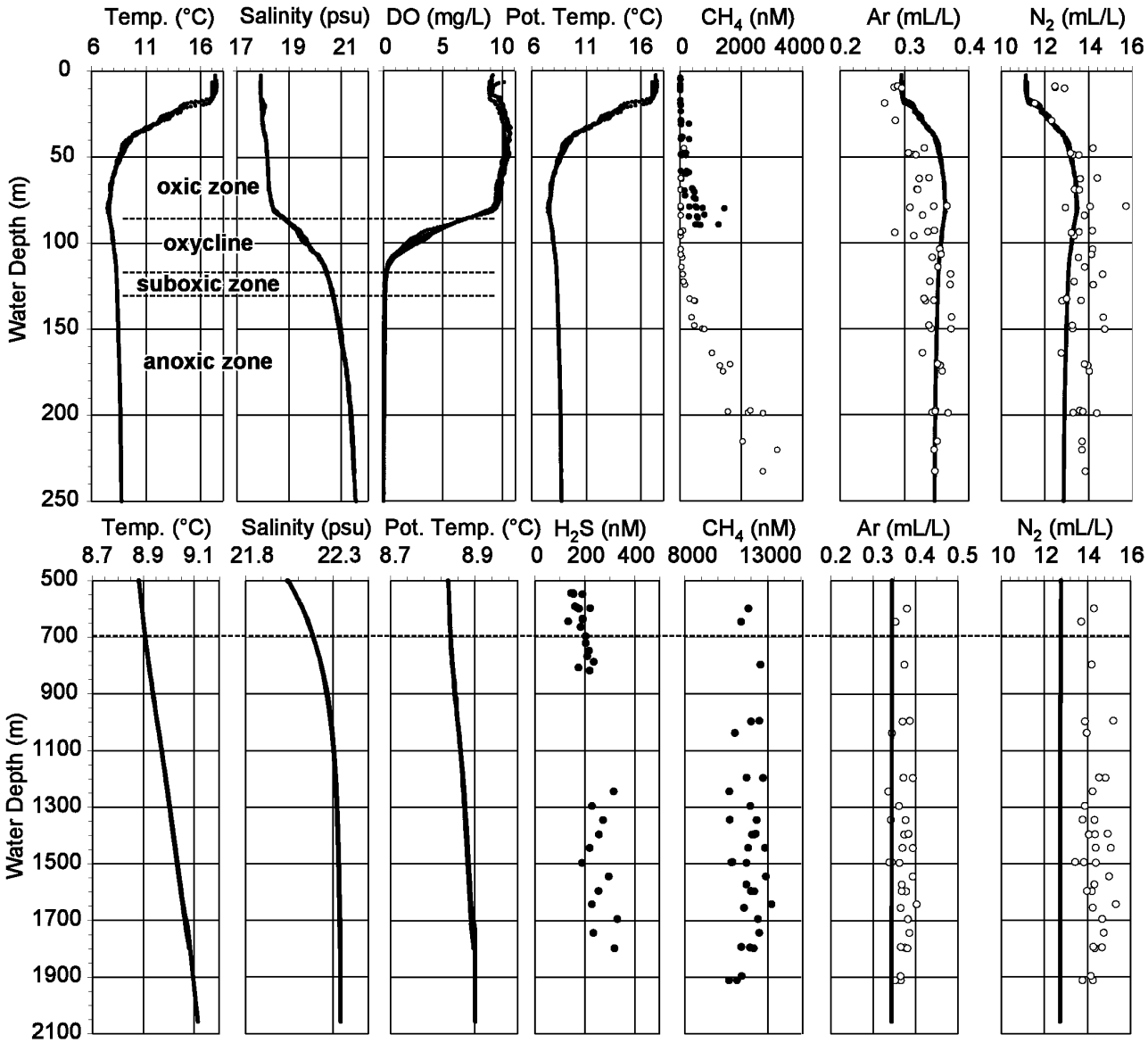

Figure 4. Conductivity-temperature-depth (CTD) and methane data from the Black Sea used for model predictions. The data at the top are from the shelf and slope in the Dnepr Paleo Delta. Black dots in the methane plot are from the shelf. Open circles in the Ar and N_2 plots are measured data; profiles are calculated from *Weiss* [1970]. The data at the bottom are from CTD stations in the Sorokin Trough. Note the well-mixed bottom boundary layer of about 300 m thickness indicated by the vertical potential temperature profile below 1800 m. The dashed line (~700 m depth) represents the phase boundary for pure methane hydrate at in situ temperature and salinity.

rates versus bubble size [*Artemov*, 2006] using a dual frequency split-beam echosounder (SIMRAD EK500, 38 and 120 kHz). Raw data from the EK500 ETHERNET output were digitally stored and processed with WaveLens software [*Artemov*, 2006]. Acoustic bubble size measurements used the relationship between target strength, frequency, depth and bubble size (TS = 10 $\log_{10}(a^2)$, with a as equivalent bubble radius [*Artemov*, 2006; *Clay and Medwin*, 1970]). As this method depends on absolute target strength values, the system was calibrated during both cruises with a 30 mm reference target [*Simrad*, 1992]. Owing to beam attenuation, bubble rising speeds and sizes are easier and more accurately acoustically measured in shallow water (<250 m).

[11] In the Dnepr Paleo Delta area, processing of the acoustic data yielded bubble diameters ranging from 1.3 to 11.3 mm, with an arithmetic mean of 4.1 mm at the 90 m seepage site. Bubble sizes within this range were confirmed during JAGO dives, TV sled and ROV observations. During one of the JAGO dives a rather constant bubble diameter of ~6 mm was observed at three different bubbling holes at the shelf, with only a few smaller bubbles (down to 1 mm) among them. The JAGO dives in general revealed sporadic release of single bubbles, a constant bubble train or several bubbles released nearly simultaneously which formed a bubble column of about 10 cm in diameter. On the basis of extensive studies throughout the entire Black Sea, *Egorov et al.* [2003]

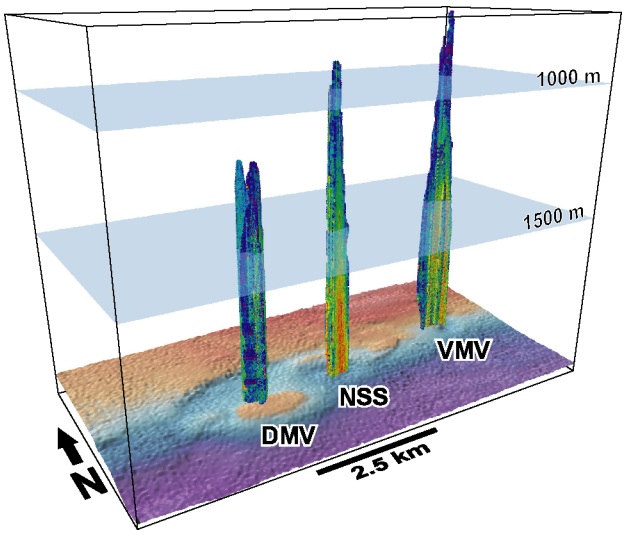

Figure 5. Perspective view of the up to 1300-m-high flares above mud volcanoes in the Sorokin Trough. At three locations, bubbles are released into the water column and rise to a water depth of up to 740 m, 45 m below the phase boundary of methane hydrate. The image shows data recorded between 9 and 12 June 2003, when all three sites, Dvurechenskiy/Vodianitskiy mud volcano (DMV/VMV) and the Nameless seep site (NSS), were active.

estimated that bubbles are in the range of 1.4 to, at most, 18.2 mm in diameter, with a mean of around 6 mm.

[12] In the Sorokin Trough, bubble release was observed above three mud volcanoes (Figure 5). The flares originate from 2065 to 2080 m water depth, and show bubble rising heights of up to 1300 m (740 m water depth). One of these sites, the Dvurechenskiy mud volcano (DMV), was previously studied in great detail during geophysical and geochemical investigations in January 2002, but no bubble release was reported [*Aloisi et al.*, 2004; *Bohrmann et al.*, 2003; *Krastel et al.*, 2003]. To date, no bubbles have been detected to rise above the HSZ (695 m water depth as calculated using the CSMHYD program of *Sloan* [1998] and a salt correction according to *Dickens and Quinby-Hunt* [1994]) at the Black Sea deep (~2000 m) sites. *Greinert et al.* [2006] provide a detailed description of the activity of the DMV and two other mud volcanoes (Figure 5) between January 2002 and August 2004. Flare heights of 1300 m above the Vodianitskiy mud volcano (VMV) have been detected several times during the CRIMEA cruises (Figures 5 and 6). Given the dense survey grid and extensive time spent above the volcanoes, the flare height (terminating at 740 m water depth) represents the top of the flare as recognizable with the echosounder system. Because of the echosounder footprint at this depth (~75 m; defined by the −3 dB lobe), the three-dimensional shape of the flare, and the slow horizontal currents in the deep Black Sea waters, *Greinert et al.* [2006] argue that it is rather unlikely that bubbles moved outside the acoustic beam during the surveys.

2.3. Iron Gate

[13] To highlight the potential for methane release from shallow, lacustrine reservoirs, such as dams during water drawdown, model runs for the Iron Gate I Reservoir (Danube River, Romania) were also performed. Unfortunately the data are rather limited and only consist of acoustic Doppler current profiler (ADCP) measurements that detected rising bubbles (Figure 1b). The ADCP (RD Instruments Workhorse 614 kHz) was attached to the boat facing downward. The boat was driven slowly (<2 km/hr) while the ADCP recorded the three-dimensional velocity components and acoustic backscatter strength within 50 cm vertical bins throughout the water column [see *McGinnis et al.*, 2006]. Physical properties of the water column were recorded with a SeaBird SBE19 and temperature loggers [*McGinnis et al.*, 2006]. Methane concentrations were assumed to be in equilibrium with the atmosphere (3.5 nM) throughout the entire water column. ADCP measurements revealed bubble rise velocities of about 25 cm/s, corresponding to a bubble diameter in the range of ~2−3 mm.

3. Gas Exchange Theory and Model

[14] The applied bubble model describes gas transfer across the surface of an individual rising bubble and tracks the dissolution and stripping of five gases, including argon, carbon dioxide, methane, nitrogen and oxygen. *Epstein and Plesset* [1950] performed one of the first studies on mass transfer from a single, static bubble. Their basic model concept has since been expanded for bubbles rising in a fluid, which has been described by various researchers [*Leifer and Patro*, 2002; *McGinnis and Little*, 2002; *Vasconcelos et al.*, 2002; *Wüest et al.*, 1992; *Zheng and Yapa*, 2002] and has been successfully applied to predict oxygen transfer from air and oxygen bubbles in various

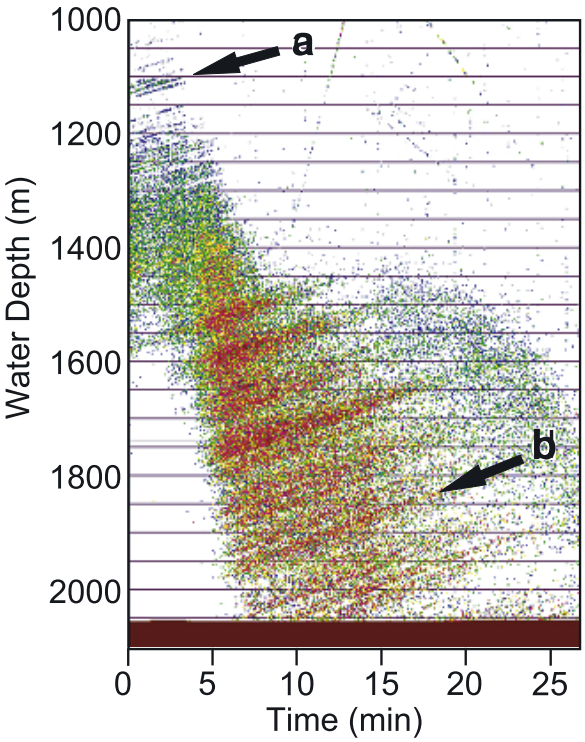

Figure 6. Echogram from the Dvurechenskiy mud volcano [*Greinert et al.*, 2006]. The arrows a and b indicate the bubbles/bubble clouds that rise at 14 and 21 cm/s, respectively.

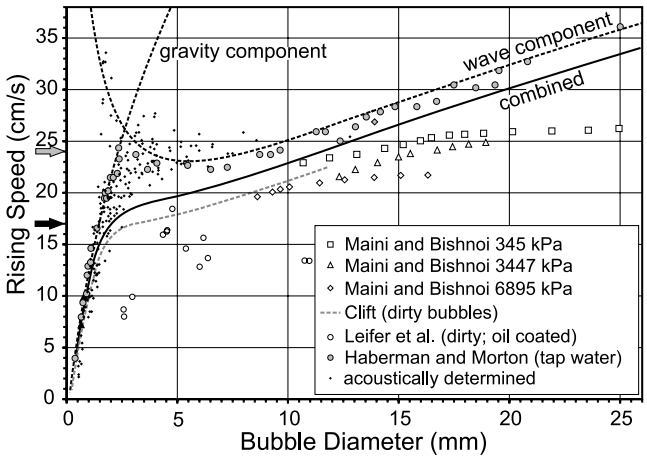

Figure 7. Measured rise velocities of bubbles with different sizes and cleanliness from various researchers. The rise velocities from *Maini and Bishnoi* [1981] are for hydrate-coated bubbles at different pressures. The acoustically determined rise velocities are from *Greinert et al.* [2006] for the Black Sea. The gray arrow along the *y* axis indicates the average rise velocity of pure gas hydrate measured by *Brewer et al.* [2002]. The black arrow indicates rise velocities of bubbles with unknown size and gas composition observed by *Merewether et al.* [1985] inside the gas hydrate stability zone. The gravity component (Stokes's law) of rise velocity is estimated by equation (2), and the wave component is predicted by equation (4) (both at 20°C). The combination of equations (2) and (4) is shown by the solid black line (combined), and this is used to calculate the rise velocity for the hydrate-rimmed bubbles.

freshwater lake oxygenation systems [*Burris et al.*, 2002; *McGinnis et al.*, 2004; *Singleton et al.*, 2006]. The major differences between the various applications of this model are the parameterizations selected for the mass transfer coefficients, rise velocities, diffusivities and solubilities.

[15] The amount of gas transferred is a function of several factors, with the most important being partial pressure, initial bubble size and bubble-water contact time. The rate of change of the amount of gas in the bubble relative to depth and gas species is given as (see Notation)

$$\frac{dM_i}{dz} = -K_{Li}(H_i P_i - C_i)\frac{4\pi r^2}{v_b}. \quad (1)$$

Note that in equation (1), K_{Li} and v_b are bubble size–dependent. The model was written in FORTRAN, and numerically integrated using the Euler method.

[16] Bubble properties, especially rise velocity and mass transfer, depend on bubble size and the presence of contaminants in the water [*Clift et al.*, 1978]. Many parameterizations exist for rise velocity and mass transfer (see *Leifer and Patro* [2002] for a thorough review of bubble experiments and theory), however those selected for this study were done so based on their simplicity and reported accuracy in the literature.

[17] As described in many studies, bubble rise velocity is affected by a wide range of naturally occurring conditions [e.g., *Alves et al.*, 2005; *Clift et al.*, 1978; *Leifer and Patro*, 2002; *Maneri*, 1995; *Zheng and Yapa*, 2000], such as clean versus dirty (i.e., absence versus presence of contaminants) or spherical versus elliptical, etc [*Clift et al.*, 1978]. The present model uses rather simple correlation equations to determine terminal rise velocities [*Jamialahmadi et al.*, 1994]. Small bubbles ($d < 2.6$ mm) are treated as rigid spheres and the terminal rise velocity can be calculated from

$$v_b = \left[\frac{4d_e g(1-\rho_G/\rho_L)}{3C_D}\right]^{1/2}, \quad (2)$$

where C_D is the drag coefficient, expressed as

$$C_D = \frac{24}{\mathrm{Re}} + \frac{3}{\sqrt{\mathrm{Re}}} + 0.34. \quad (3)$$

Figure 7 shows that equation (2) predicts reasonably well the tap water data up to a bubble diameter of $d = 2.6$ mm. Larger bubbles, however, experience surface oscillations and the rise of the bubble can be compared to a wave traveling in an ideal fluid [*Jamialahmadi et al.*, 1994]. On the basis of this wave analogy the rise velocity of larger bubbles can be predicted by

$$v_b = \sqrt{\frac{2\sigma}{d(\rho_L+\rho_G)} + \frac{gd}{2}}. \quad (4)$$

Combining the above equations [see *Jamialahmadi et al.*, 1994] provides a good approximation for the rise velocity of dirty bubbles, predicting rising speeds which are similar, but slightly faster, than those proposed by *Clift et al.* [1978] (Figure 7).

[18] Like bubble rise velocity, gas transfer across the bubble surface is also affected by many factors, including bubble size, internal gas circulation, rise velocity and surfactants [*Alves et al.*, 2005; *Clift et al.*, 1978; *Leifer and Patro*, 2002; *Vasconcelos et al.*, 2002, 2003]. For deep water bubble releases, *Zheng and Yapa* [2002] combine three equations for K_{Li} (m/s) based on those developed by *Clift et al.* [1978] and *Johnson et al.* [1969]:

$$K_{Li} = 1.13\left(\frac{v_b}{0.45+0.2d_e}\right)^{1/2} D_i^n, \quad d_e \text{ from 0 to 0.5 cm}, \quad (5)$$

$$K_{Li} = 6.5 D_i^n, \quad d_e \text{ from 0.5 to 1.3 cm}, \quad (6)$$

$$K_{Li} = 6.94 d_e^{-1/4}, \quad d_e > 1.3 \text{ cm}, \quad (7)$$

where the diffusion coefficient D is in cm^2/s, v_b is in cm/s and d_e is in cm. The diffusion exponent, n, varies from 1/2 to 2/3 for clean bubbles and dirty bubbles, respectively [*Jähne et al.*, 1987; *Leifer and Patro*, 2002]. *Zheng and Yapa* [2002] demonstrate that these correlations fit reasonably well with literature data for CO_2 and O_2 for $n = 1/2$. The diffusion coefficient D (cm^2/s) is taken as [*Hayduk and Laudie*, 1974]

$$D_i = \frac{13.26\times10^{-5}}{\mu^{1.14} V_i^{0.589}}, \quad (8)$$

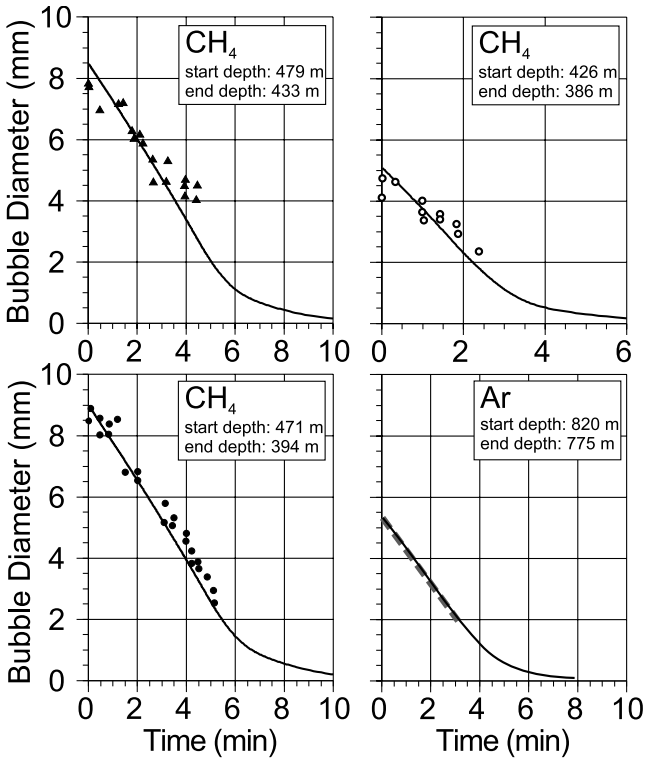

Figure 8. Model results for data presented by *Rehder et al.* [2002] for bubble dissolution above the hydrate stability zone (HSZ). The dashed line on the argon plot represents the argon dissolution data from *Rehder et al.* [2002].

where μ is in centipoises and V_i is expressed in cm^3/mol. Values used for V_i are obtained from *Hayduk and Laudie* [1974].

[19] To account for pressure effects at great depths, the Peng-Robinson equation of state is used to calculate gaseous properties [*Peng and Robinson*, 1976]. The modified Henry's equation is used to account for the solubility and fugacity of nonideal gases at high pressure [*King*, 1969; *Schmid et al.*, 2003]. The salinity effect on solubility was estimated from *Weiss* [1974]. The Henry's coefficients for nitrogen and oxygen are the same as used by *Wüest et al.* [1992], argon is taken from *Wilhelm et al.* [1977] and carbon dioxide and methane from *Weiss* [1974] and *Rettich et al.* [1981], respectively.

4. Model Application and Calibration for Gas Hydrate-Rimmed Bubbles

[20] The model is compared to data collected by *Rehder et al.* [2002], who released methane bubbles in Monterey Bay at water depths between 430 to 820 m, both within and above the HSZ. These data are used to calibrate the model to describe bubble dissolution within the HSZ.

4.1. Above the Hydrate Stability Zone: Monterey Bay

[21] The phase boundary for pure methane hydrate in Monterey Bay is at about 520 m at ambient temperature and salinity [*Rehder et al.*, 2002]. During their experiments *Rehder et al.* [2002] monitored bubble dissolution with an ROV as the bubble rose and measured bubble shrinkage by video observation. Because of the oxic conditions, and the fact that they also released argon bubbles, the model includes gaseous and dissolved argon, carbon dioxide, methane, nitrogen and oxygen.

[22] The initial bubble size for each model run was determined using the best model fit with the data at various initial depths (Figure 8) and predicts dissolution well for both methane and argon bubbles. Discrepancies between the data and model results are likely due to surfactants inhibiting the mass transfer, as surface contamination has been shown to generally increase with bubble age [*Alves et al.*, 2005] and decreasing bubble diameter [*Vasconcelos et al.*, 2002]. In all model runs the bubble diameter decreases almost linearly until the bubble diameter is smaller than about 2 mm. Below this size (after ~6 min) the dissolution rate decreases further as a result of a more rapidly diminishing value for mass transfer (K_{Li}). However, these model simulations assume a clean bubble (no surfactants; $n = 1/2$ in equations (5) and (6)). Bubble dissolution would be much slower if the bubble surface became immobile due to contaminants. Therefore given the wide range of parameters that affect dissolution, the measured data and model results appear to match reasonably well for this deep, saline, oxic system.

4.2. Within the Hydrate Stability Zone: Monterey Bay

[23] *Rehder et al.* [2002] also released methane bubbles within the HSZ and their results support the widely accepted assumption of a hydrate rim formation, which severely inhibits mass transfer. This is indicated by a 12% slower initial dissolution rate of methane bubbles released within the HSZ (12.8 μm/s) compared to those released above it (15.5 ± 3.2 μm/s). For bubble diameters below 2.7–4 mm the dissolution rate decreased again to an average of only 3.0 μm/s, as the bubble surface was "frozen" (Figure 9). This effect was not seen with argon bubbles, which do not form hydrates at the release depth and temperature conditions in Monterey Bay (neglecting salinity contributions, the argon hydrate phase boundary is ~1270 m according to *Marshall et al.* [1964]). As an additional indication of increasing surfactants (gas hydrate crystals) at the bubble surface, *Rehder et al.* [2002] observed that the bubble shape and path oscillations were dampened for methane bubbles inside the HSZ.

4.3. Hypothesis of Methane Hydrate Rim Formation

[24] While fairly extensively studied [*Gumerov and Chahine*, 1998; *Maini and Bishnoi*, 1981; *Rehder et al.*, 2002; *Topham*, 1984a, 1984b], the nature of hydrate formation around bubbles is not yet fully understood. Hydrate formation from trapped bubbles within the HSZ [*Brewer et al.*, 2002] and the kinetics of rim formation on bubbles has been reported to be extremely rapid [*Maini and Bishnoi*, 1981; *Topham*, 1984a]. The slower dissolution of bubbles below the HSZ from the very beginning of the experiments by *Rehder et al.* [2002] also points to immediate hydrate formation. Therefore it can be suggested that nucleation occurs immediately and that successive hydrate crystallization finally forms a complete rim, creating a "frozen bubble." The different stages might be as follows (Figure 10).

[25] 1. Gas hydrate formation occurs immediately as the bubble enters the water column, and may even be formed in

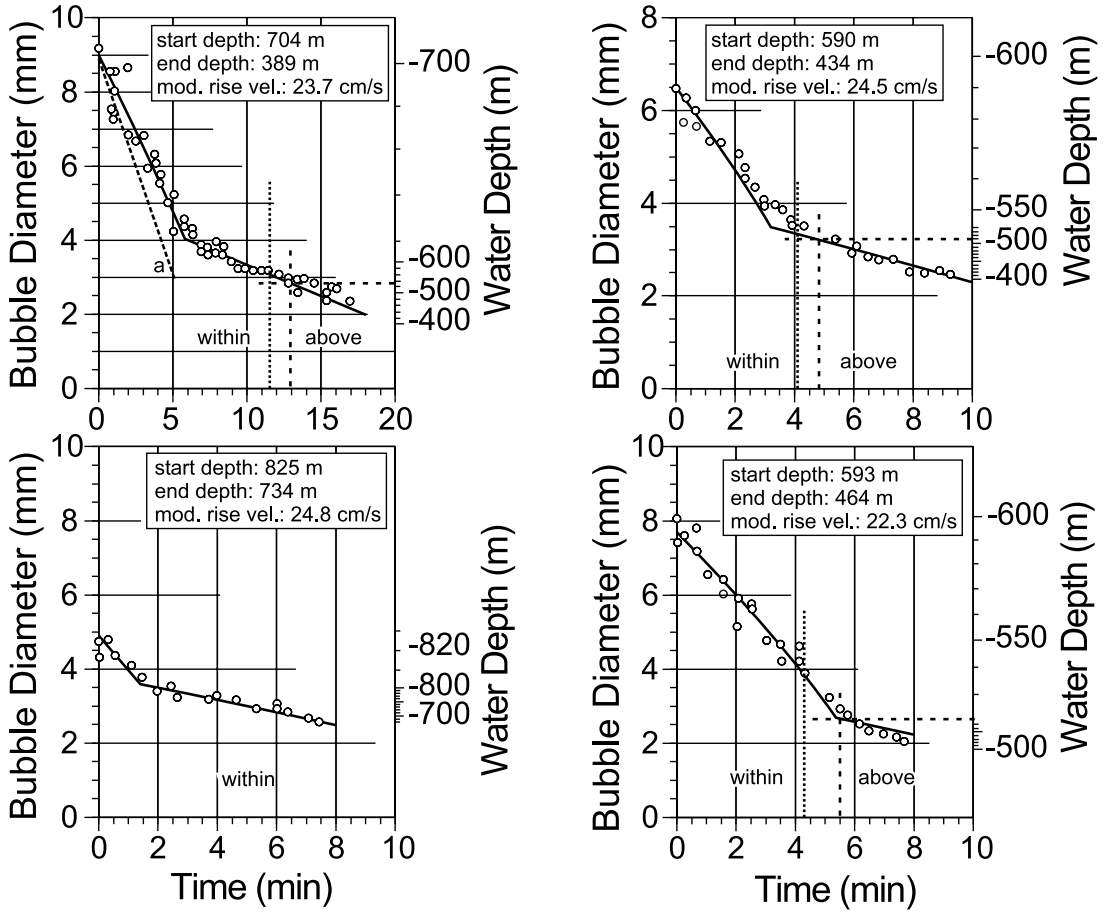

Figure 9. Results of the calibrated gas hydrate rim model for bubbles released inside the HSZ as obtained from *Rehder et al.* [2002]. Dashed line a in the upper left panel shows the shrinking rate of methane bubbles above the HSZ. The depth axis is drawn with respect to the modeled rise velocity as given. This rise velocity is slower than the real rising of the bubbles during the experiment (~28.5 cm/s). Thus in reality the bubbles were above the HSZ (left dotted lines) earlier than calculated with the modeled rising speed (dashed crossing lines). It is obvious that no significant change in the bubble behavior occurs at the ambient hydrate phase boundary. The given start and end depths are those measured during the experiment (G. Rehder, personal communication, 2005).

the sediment. The surface may remain partially mobile due to shear stress but internal gas circulation is already reduced, resulting in the ~12% lower mass transfer observed by *Rehder et al.* [2002]. Formed hydrate particles are swept to the downstream side of the bubble, leaving the upstream side relatively clean. This Marangoni effect inhibits surface motion and decreases both the rise velocity and mass transfer [*Clift et al.*, 1978; *Leifer and Patro*, 2002; *Vasconcelos et al.*, 2002].

[26] 2–3. As the bubble dissolves and hydrate formation continues, the shear across the surface is reduced resulting in an ever-increasing density of hydrate particles on the bubble. Large enough bubbles may still oscillate at this time.

[27] 4. At some point the bubble becomes small enough, or the hydrate formation driving force is high enough, that the tensile strength of the hydrate structure overcomes the shear stress on the bubble surface due to the rise velocity. A complete hydrate rim forms evoking the no-slip boundary conditions, or rigid sphere. The point (time/bubble size) at which this occurs depends on the hydrate formation driving force (speed of hydrate crystallization), i.e., the depth, temperature, partial pressure of methane within the bubble and ambient methane concentrations. This dependency between pressure (depth), bubble size and the beginning of the frozen bubble/rigid sphere behavior was recently observed by *Rehder et al.* [2005]. For the data shown here [*Rehder et al.*, 2002], this "freezing point" occurs when the bubbles are about 2.7–4 mm in diameter, which is in close agreement with the observations of *Vasconcelos et al.* [2002] for transitioning between clean and dirty bubbles. In laboratory tests, stationary methane bubbles at high pressures formed a hydrate rim very rapidly, however the bubble collapsed within tens of seconds due to internal methane consumption for hydrate formation and the resulting pressure drop [*Gumerov and Chahine*, 1998]. This collapse was also observed by *Maini and Bishnoi* [1981] at constant pressures in laboratory tests. It is thought that in nature, the internal pressure drop due to hydrate formation is compensated for by decreasing hydrostatic pressure as the rimmed bubble rises, allowing a long bubble life. As the hydrate dissociates on the outside, new hydrate is formed on the inside of the rim. It has been suggested that the

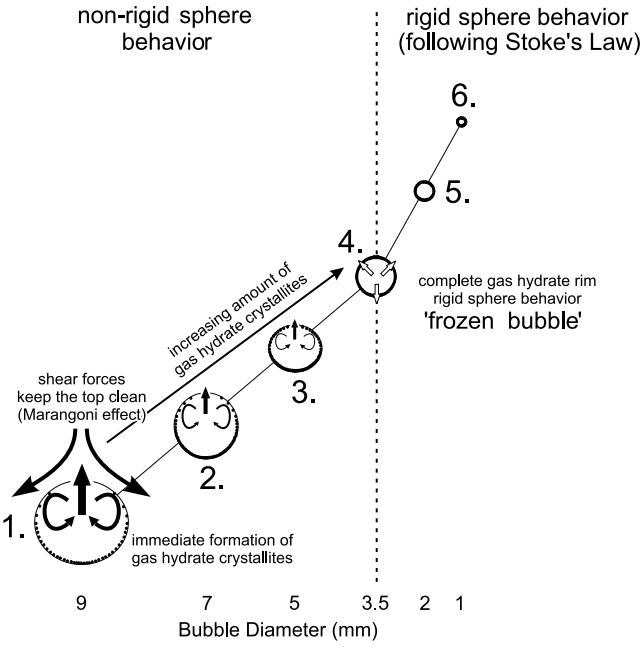

Figure 10. Proposed hydrate rim formation on bubbles during their rise, with a complete gas hydrate rim forming a frozen bubble at 3.5 mm size.

necessary water supply for the internal hydrate formation is provided via capillary action across the bubble surface [*Topham*, 1984a]. This action of hydrate dissociation/formation keeps the bubble from expanding very rapidly as it rises, and minimizes cracks and surface mobilization.

[28] 5–6. The subsequent drastically reduced bubble dissolution rate enables the bubble to rise high in the water column. Bubbles even remain "frozen" when passing the HSZ boundary (Figure 9) (G. Rehder, personal communication, 2005). The reason for this is unknown, but one can speculate that the endothermic hydrate decomposition may cool down the temperature within the diffusive boundary layer surrounding the bubble, creating a microenvironment that keeps the gas hydrate stable.

4.4. Model Calibration for Gas Hydrate-Rimmed Bubbles

[29] Despite the knowledge gap of what exactly happens to the methane bubble within the HSZ, the model was calibrated to account for the freezing point at bubble diameters between 2.7 and 4 mm, after which mass transfer is severely inhibited. The model was first fit to the initial dissolution curve before the bubble becomes frozen by slightly increasing the diffusion exponent from $n = 1/2$ to 0.52 in equations (5) and (6), which accounts for increasing bubble "dirtiness" due to the accumulating hydrate particles on the bubble surface. For complete rim formation, n was increased to 2/3 (equations (5) and (6)) for bubbles smaller than 2.7–4 mm in diameter.

[30] Calibration resulted in good fits with the data (Figure 9). The difference in "freezing" points may be due to the different release conditions, surrounding dissolved methane concentrations or other gases present in the bubble. The transition (freezing point) time and corresponding diameter from clean to dirty bubbles is suggested by *Vasconcelos et al.* [2002] to be a function of initial bubble diameter and gas concentrations. The freezing times and diameters observed by *Rehder et al.* [2002] are indeed in general agreement with the observations of *Vasconcelos et al.* [2002] for transitioning from clean to dirty bubbles. Furthermore, the changeover from clean ($n = 0.52$) to dirty bubble behavior ($n = 2/3$) is rather abrupt, as observed by *Jähne et al.* [1987].

5. Model Application for the Black Sea

[31] Three different areas were chosen to model bubble rise. Two sites are from the Dnepr Paleo Delta (90 and 230 m water depth), while the third is from the Sorokin Trough (>2000 m water depth).

5.1. Above the Hydrate Stability Zone: Dnepr Area 90 m

[32] The model was used to back calculate the initial bubble size necessary to result in bubbles acoustically observed in different water depths (Figure 11). According to the model results a bubble having a diameter of about 0.8 mm at 13 m depth would have been released as a 5.5 mm bubble at 90 m (curve A in Figure 11). Although this bubble would reach the sea surface with a diameter of about 1 mm, the gas fraction of nitrogen and oxygen approaches atmospheric levels and all the methane is dissolved. Similarly, 6–8 mm diameter bubbles in about 60 m depth would require an initial diameter of 8.5 mm and would be 7 mm in diameter at the surface. While the mole fraction of methane in such bubbles would still be 35%, only ~2% of the original mass of methane remains. Acoustic (Figure 12) and visual observations reveal that bubbles of up to ~10 mm diameter do indeed reach the sea surface at the 90 m site.

[33] The entire range of modeled initial bubble sizes (between ~2 and 9 mm) agrees well with the acoustically and visually determined size range of 1.3 to 11.3 mm. The three model results in Figure 11, showing initial bubble sizes between 4 and 6 mm and thus close to the rather narrow size range observed during a JAGO dive, reasonably support the accuracy of the model. However, as there were only three detailed observations from JAGO, this may not be statistically significant.

5.2. Above the Hydrate Stability Zone: Dnepr Area 230 m

[34] Massive releases of large bubbles (>10 mm in diameter) at the 230 m site are described by *Michaelis et al.* [2002], and acoustic data show that a few flares even rise up to the sea surface (Figures 1a and 12). The model predicts that a 12.4 mm diameter bubble would be required to just reach the sea surface (Figure 13). A bubble of ~20 mm diameter, on the uppermost observed size limit, would still be 20 mm when it reaches the surface, but the amount of methane remaining would be much less than 1% of its original mass. However, bubbles this large may have a tendency to break apart during their rise and are transported as smaller bubbles with faster dissolution and gas exchange.

5.3. Within the Hydrate Stability Zone: Sorokin Trough 2080 m

[35] The model was applied with and without the gas hydrate rims to better understand the very tall flares ob-

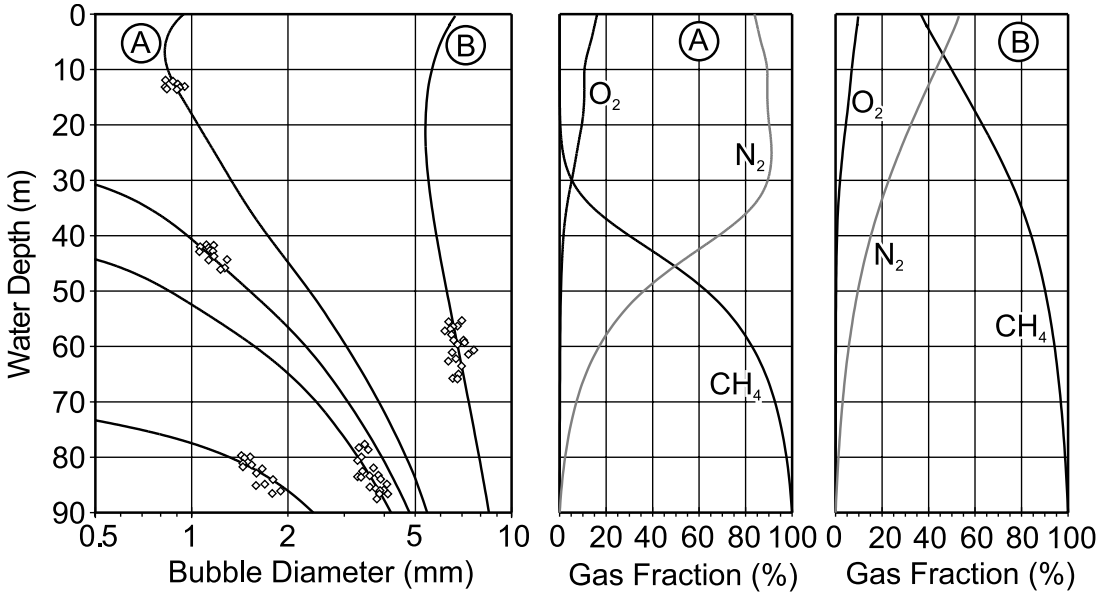

Figure 11. Model runs that fit acoustically observed bubbles (open diamonds) in different water depths (note that the left graph has a logarithmic x scale). The changing gas composition of bubbles A and B shows that the smaller bubble A (d_o = 5.5 mm) does not contain any more methane upon reaching the surface, whereas bubble B (d_o = 8.5 mm) is still composed of 35% methane, although only 2% of the original mass remains due to dissolution.

served in the Black Sea (Figures 5 and 6). Model runs were conducted to determine (1) the initial bubble size required to reach the observed flare height and (2) the hypothetical initial bubble diameter required to reach the sea surface. The physical and geochemical boundary profiles for the Sorokin Trough are shown in Figure 4. In terms of bubble transport, H_2S and CO_2 are considered negligible, as both compounds are highly soluble and neither comprises more than about 0.01% of the bubble molar fraction in model predictions.

[36] Model runs assuming no hydrate rim predict that it would require at least a 40 mm diameter bubble released at 2080 m to rise a distance of 1300 m, i.e., the top of the observed flares; a hypothetical 50 mm diameter bubble would rise to the sea surface (Figure 14). Such large bubbles are unlikely to exist and would break apart.

[37] Assuming a complete hydrate rim exists at 3.5 mm diameter, a 20 mm diameter bubble would be needed to rise 1300 m. While not entirely impossible, it still seems highly unlikely that such large bubbles would be continuously formed. However, if a complete rim formation is immediate (frozen stage from the very beginning), a bubble having a diameter of only 9 mm would rise a distance of 1300 m (Figure 14). The 9 mm bubble is much more realistic and would not break apart. It should be pointed out that 1300 m is an exceptionally high flare in the Black Sea. A 6 mm bubble diameter (a likely mean value) would in fact still rise 800 m, which corresponds well to the Dvurechenskiy mud volcano flare [*Greinert et al.*, 2006]. The measured rising speeds of 21 cm/s at the base and 14 cm/s at the top of the flare shown in Figure 6 indicate bubble sizes in the range of 9.5 mm at the base to 1.3 mm at the top. The model results for hydrate-rimmed bubbles compare well with these sizes. As we never observed bubble rising rates well above 25 cm/s during our acoustic observations, we can rule out the existence of a two-phase plume with significantly increased rise velocities.

[38] Model simulations also show that an ~11 mm diameter rimmed bubble would travel 2080 m and reach

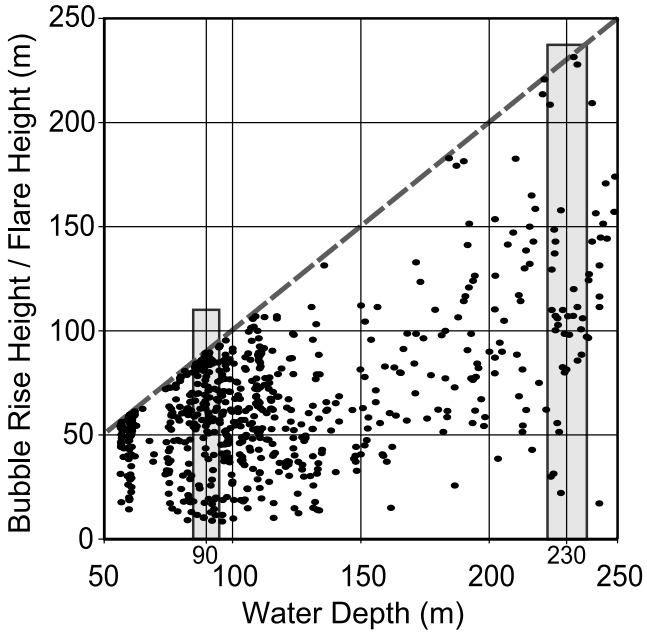

Figure 12. Acoustically detected bubble rising height/flare height along the shelf and slope of the Dnepr Paleo Delta area. Dots on the gray dashed line (1:1 line) represent bubbles that reached the sea surface [*Egorov et al.*, 2003]. The depth range for the two areas discussed here is marked in gray.

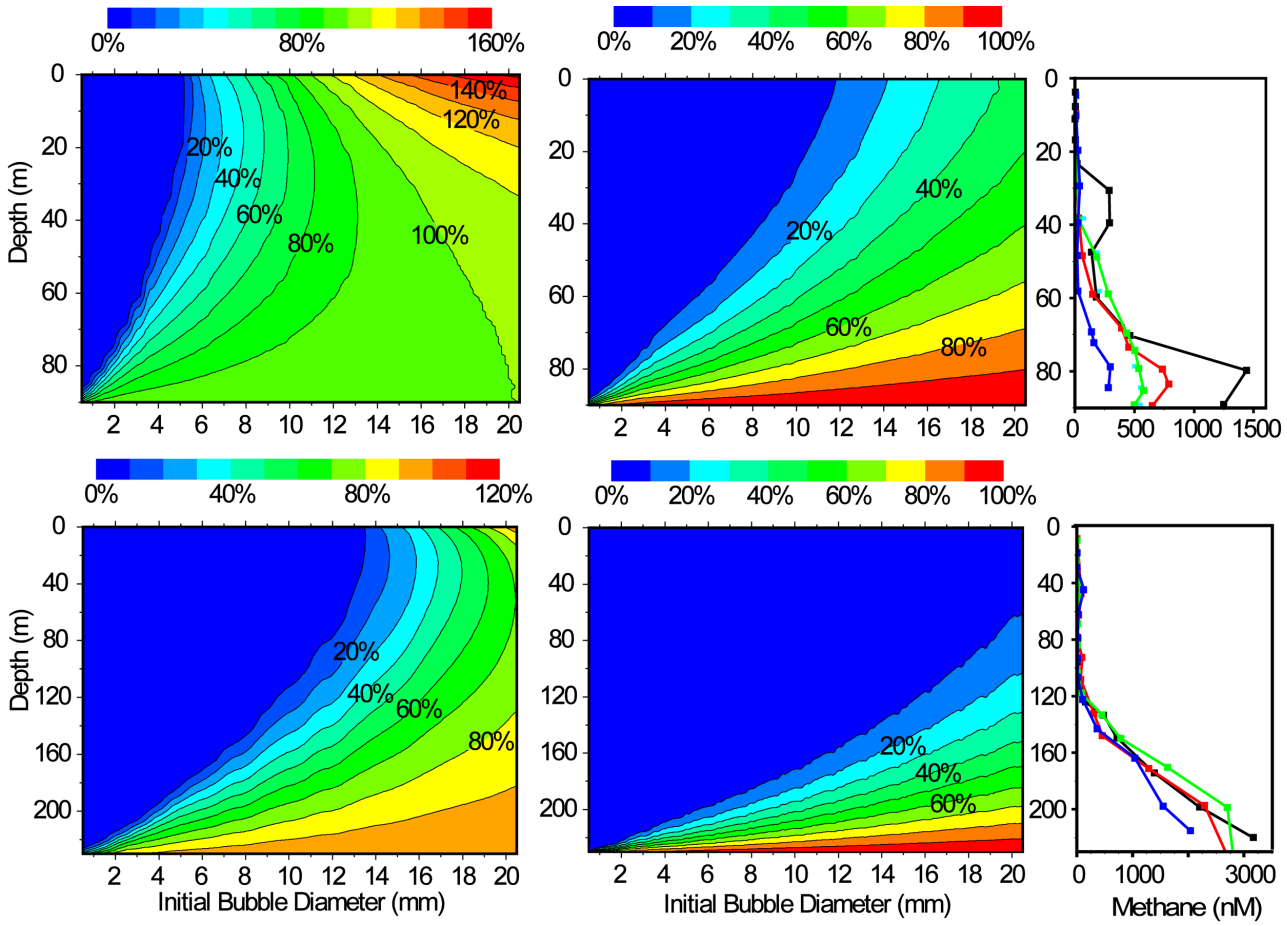

Figure 13. Modeled fate of methane bubbles of different sizes at the 90- and 230-m-deep sites in the Dnepr Paleo Delta area. (left) Percent of the original bubble volume with depth. (middle) Percent of the original methane remaining in the bubble. At the 90-m-deep site, a bubble that still contains 10% of methane must have been released as a 12 mm bubble (top middle). At the surface, the bubble itself would be even larger (110%) compared to its initial size (top left). (right) The measured dissolved methane concentrations indicate that, indeed, most of the bubble methane is dissolved close to the seafloor.

the water surface. It should be remembered, however, that this simulation assumes that the hydrate rim will remain until the water surface. While *Rehder et al.* [2002] observed that the hydrate rim appeared to remain for some time after passing the HSZ boundary (Figure 9), this would disappear well below the water surface, resulting in total dissolution much earlier than that predicted.

6. Methane Reaching the Atmosphere

[39] Black Sea methane flares and bubble observations are compared with model predictions to identify the critical boundary conditions for methane venting to the atmosphere. As already evident from section 5, the bubbles will only reach the surface in the shallow sites, and in most cases a significant portion of the methane has already been dissolved in the water column. The model is further applied to the Iron Gate I dam, a shallow, freshwater body, to demonstrate not only the growing concern toward dams and lakes as greenhouse gas contributors, but also to estimate the contribution of very shallow seeps in the Black Sea or other water bodies.

6.1. Black Sea

[40] Figure 13 shows model results for various bubble sizes released at 90 and 230 m water depth, together with concentration profiles of dissolved methane. As an example, an 11 mm bubble released in 90 m would also be 11 mm when it reached the sea surface but would contain only about 5% of its initial mass of methane. It is obvious from Figure 13 that most of the methane from bubbles is rapidly dissolved in the water close to the seafloor (a few tens of meters), resulting in higher methane concentrations near the seafloor. Once methane is dissolved, vertical transport is limited to turbulent diffusion, which has been shown to be slow in the Black Sea [*Gregg and Yakushev*, 2005]. This means that bubbles do not transport/dissolve significant amounts of methane into the surface mixed layer in the Black Sea (~40 m water depth [*Stanev et al.*, 2004]). Thus even from high-intensity seep sites, direct methane transport by bubbles into the atmosphere is very small for the observed bubble release conditions (no plume scenario) and sizes. For bubbles released in 230 m deep water, it is almost impossible to transport methane into the atmosphere.

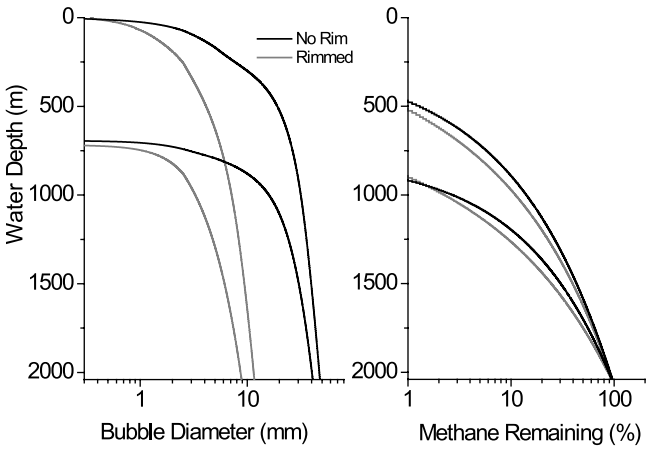

Figure 14. Model runs for the observed flare height above the mud volcanoes in the Sorokin Trough, rising up 1300 m to a depth of ~700 m. A 9 mm bubble, on which a gas hydrate rim is formed immediately, would rise this distance, whereas a 40 mm nonrimmed bubble would be required to rise the same distance. Similarly, an 11 mm hydrate-rimmed bubble would reach the surface (with the unrealistic assumption that the rim did not dissociate above the HSZ), and an almost 50 mm nonrimmed bubble would be required to rise the same distance.

These model results are supported by dissolved methane concentrations at the Black Sea surface and flux calculations between the water and atmosphere presented by *Schmale et al.* [2005]. The authors measured slightly enriched methane concentrations at the surface only above seep sites with depths <100 m.

6.2. Iron Gate I Reservoir

[41] More concern should be given to methane release from shallow lakes or water reservoirs, such as Iron Gate I as a typical representative. Assuming that the bubbles released from the sediment shown in Figure 1b are pure methane, a 1 mm diameter bubble is required to reach the surface from 23 meter deep water, and a 6 mm bubble will still have about 30% of its original amount of methane when it reaches the surface. Additionally, in the case of Iron Gate I, methane dissolved in the water column will be released to the atmosphere through turbine discharges. In fact, most of the methane in the Iron Gate I water column will reach the atmosphere as reservoir stratification is very weak due to high-flow conditions and frequent diurnal turnovers [*McGinnis et al.*, 2006]. While the simulations are run with slightly different (freshwater) conditions, the results are very similar to those shown in Figure 15. Thus as a first approximation, model predictions presented in this figure can be used to evaluate which bubble size would contribute "significantly" to direct methane transport to the atmosphere.

7. Summary and Conclusions

[42] A single bubble model was developed that accounts for salinity and pressure effects on gas solubility and nonideal gas properties. The model was applied to a wide range of environmental conditions in the ocean (low to high salinity, oxic to anoxic) using published observations from Monterey Bay [*Rehder et al.*, 2002] and data obtained in this study from the Black Sea. The model tracks the dissolution and stripping of Ar, CH_4, CO_2, N_2 and O_2 in bubbles, and predicts changing bubble size, gas composition and rising speed.

[43] The model provides good predictions of the experimental data for methane and argon bubbles in Monterey Bay above the hydrate stability zone, and was calibrated to fit the observed decreased methane bubble dissolution rate within the hydrate stability zone. It is assumed that the initial decrease of about 12% in the bubble dissolution rate is due to the immediate formation of gas hydrate crystals on the bubble surface. A complete gas hydrate coating then "freezes" the bubble surface and drastically reduces its dissolution rate to only 20% of its initial (ordinary, nonrimmed) value. During the experiments of *Rehder et al.* [2002], this occurred at bubble sizes between 2.7 to 4 mm in diameter, but will likely occur faster and at larger diameters with increasing depth and background methane concentrations. Further experiments are required to fully understand and model the processes involved in the formation of hydrate rims and their effects on bubble stability.

[44] Modeling results from three Black Sea sites were in good agreement with visual and acoustic observations. The model shows how the immediate formation of a hydrate rim on bubbles of physically feasible sizes (i.e., 6 to 9.5 mm diameter) in 2000 m deep water can explain the exceptionally high flares observed to rise 800 to 1300 m above mud volcanoes in the Sorokin Trough. Acoustically measured bubble rising speeds of 21 cm/s at the flare base and 14 cm/s at the flare top indicate bubble sizes of 9.5 and 1.3 mm respectively, which fits well with the model predictions. Model runs at a 90 m and 230 m deep seep site also yielded bubble sizes in good agreement with acoustically measured sizes in different depths. Results from the 230 m site indicate that methane release to the atmosphere from these seeps is unlikely.

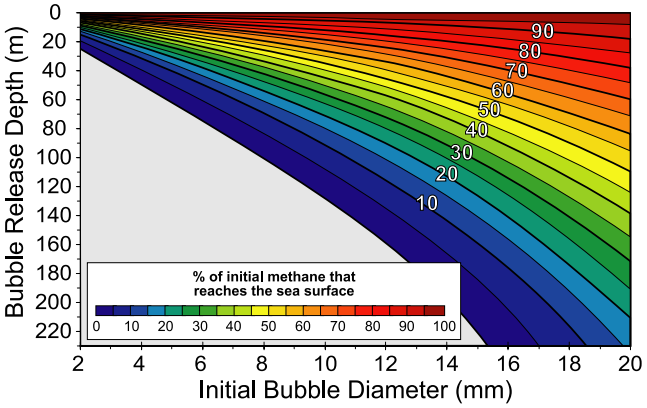

Figure 15. Contour plot of the percentage of the initial methane mass reaching the atmosphere as a function of initial bubble diameter and release depth (methane reaching the surface is read at the point where the bubble diameter and release depth intersect on the plot). Environmental conditions were those from the Black Sea; however, these results are also valid as a first approximation for "normal" open ocean (e.g., Monterey Bay) or lake/reservoir conditions.

[45] Using the model and observations in this work it becomes obvious that significant methane transfer to the atmosphere is only possible from very shallow water depths, i.e., less than 100 m. This is in good agreement with surface water methane concentrations presented by *Schmale et al.* [2005], who show elevated concentrations only above seep areas at the shelf (<100 m).

[46] Of course the amount of methane that reaches the atmosphere due to bubble transport depends on initial bubble size, bubble release depth and if massive release causes the formation of a bubble plume. However, in most cases and even if a bubble reaches the surface with a significant size, most of the methane is dissolved into the water column and replaced by other stripped gases, particularly oxygen (in oxic conditions) and nitrogen. Therefore only a catastrophic bubble release will contribute significantly to the direct methane transport from deep water seeps (>100 m) to the atmosphere.

[47] These conclusions can be applied to other stratified systems, because the results are qualitatively similar within the range of temperature, salinity and gas concentrations commonly observed in natural systems. Lakes and hydropower reservoirs may be significant contributors, as they are often shallow, and methane can reach the atmosphere through turbine discharges from dams, overturn events or bubble dissolution into the surface mixed layer.

Notation

C aqueous phase concentration, mol/m^3.
C_D drag coefficient.
d bubble diameter, m, cm, mm.
D diffusion coefficient, cm^2/s.
g gravitational constant, m/s^2.
H Henry's constant, mol/(m^3 bar), bar/(mol m^3).
K_L liquid-side mass transfer coefficient, m/s.
M mass of gaseous species, mol.
P pressure, bar, Pa.
r bubble radius, m.
Re Reynolds number.
v velocity, m/s, cm/s.
V molar volume, cm^3/mol.
z depth, m.
μ dynamic viscosity, kg/(m s).
ρ density, kg/m^3.
σ interfacial surface tension, N/m.

Subscripts and superscripts
b bubble.
e equivalent.
G gas.
i individual, partial.
L liquid.
n diffusion exponent.

[48] **Acknowledgments.** The authors express their deepest gratitude to the captain and crew of the R/V *Professor Vodyanitskiy*. We would further like to thank all partners of the CRIMEA ("Contribution of high-intensity gas seeps in Black Sea to the methane emission to the atmosphere") project for their support. Gas sampling and direct bubble observation were undertaken during a cruise within the EU-funded METROL project which J. Greinert could join, and thus our thanks go to C. Borowski and B. Joergensen, who gave us this opportunity. We thank G. Rehder for supplying unpublished data from his experiments. We also thank M. Schmid and two anonymous reviewers for their improvements to the manuscript. Financially, the project was supported by the EC project EVK-2-CT-2002-00162 (CRIMEA). The first author was also supported by the Swiss National Science Foundation (grant 200020-103827.1).

References

Adams, D. D. (2005), Diffusive flux of greenhouse gases—methane and carbon dioxide—at the sediment-water interface of some lakes and reservoirs of the world, in *Greenhouse Gas Emissions: Fluxes and Processes, Hydroelectric Reservoirs and Natural Environments*, edited by A. Tremblay et al., pp. 129–153, Springer, New York.

Aloisi, G., M. Drews, K. Wallmann, and G. Bohrmann (2004), Fluid expulsion from the Dvurechenskii mud volcano (Black Sea)—part I. Fluid sources and relevance to Li, B, Sr, I and dissolved inorganic nitrogen cycles, *Earth Planet. Sci. Lett.*, *225*, 347–363.

Alves, S. S., S. P. Orvalho, and J. M. T. Vasconcelos (2005), Effect of bubble contamination on rise velocity and mass transfer, *Chem. Eng. Sci.*, *60*, 1–9.

Artemov, Y. G. (2006), Software support for investigation of natural methane seeps by hydroacoustic method, *Mar. Ecol. J.*, *5*, 57–71.

Bastviken, D., J. Cole, M. Pace, and L. Tranvik (2004), Methane emissions from lakes: Dependence of lake characteristics, two regional assessments, and a global estimate, *Global Biogeochem. Cycles*, *18*, GB4009, doi:10.1029/2004GB002238.

Bohrmann, G., et al. (2003), Mud volcanoes and gas hydrates in the Black Sea: New data from Dvurechenskii and Odessa mud volcanoes, *Geo Mar. Lett.*, *23*, 239–249.

Brewer, P. G., C. Paull, E. T. Peltzer, W. Ussler, G. Rehder, and G. Friederich (2002), Measurements of the fate of gas hydrates during transit through the ocean water column, *Geophys. Res. Lett.*, *29*(22), 2081, doi:10.1029/2002GL014727.

Buffett, B. A. (2000), Clathrate hydrates, *Annu. Rev. Earth Planet. Sci.*, *28*, 477–507.

Burris, V. L., D. F. McGinnis, and J. C. Little (2002), Predicting oxygen transfer rate and water flow rate in airlift aerators, *Water Res.*, *36*, 4605–4615.

Cicerone, R. J., and R. S. Oremland (1988), Biogeochemical aspects of atmospheric methane, *Global Biogeochem. Cycles*, *2*, 299–327.

Clay, C. S., and H. Medwin (1970), Dependence of spatial and temporal correlation of forward-scattered underwater sound on surface statistics. 1. Theory, *J. Acoust. Soc. Am.*, *47*, 1412–1418.

Clift, R., J. R. Grace, and M. E. Weber (1978), *Bubbles, Drops, and Particles*, 380 pp., Elsevier, New York.

Dando, P. R., P. Jensen, S. C. M. O'Hara, S. J. Niven, R. Schmaljohan, U. Schuster, and L. J. Taylor (1994), The effects of methane seepage at an intertidal/shallow subtidal site on the shore of the Kattegat, Vendsyssel, Denmark, *Bull. Geol. Soc. Den.*, *41*, 65–79.

De Batist, M., J. Klerkx, P. Van Rensbergen, M. Vanneste, J. Poort, A. Y. Golmshtok, A. A. Kremlev, O. M. Khlystov, and P. Krinitsky (2002), Active hydrate destabilization in Lake Baikal, Siberia?, *Terra Nova*, *14*, 436–442.

Dickens, G. R., and M. S. Quinby-Hunt (1994), Methane hydrate stability in seawater, *Geophys. Res. Lett.*, *21*, 2115–2118.

Egorov, V. N., G. G. Polikarpov, S. B. Gulin, Y. G. Artemov, N. A. Stokozov, and S. K. Kostova (2003), Present-day views on the environment-forming and ecological role of the Black Sea methane gas seeps (in Russian), *Mar. Ecol. J.*, *5*, 5–26.

Epstein, P. S., and M. S. Plesset (1950), On the stability of gas bubbles in liquid-gas solutions, *J. Chem. Phys.*, *18*, 1505–1509.

Granin, N. G., and L. Z. Granina (2002), Gas hydrates and gas venting in Lake Baikal, *Russ. Geol. Geophys.*, *43*, 629–637.

Gregg, M. C., and E. Yakushev (2005), Surface ventilation of the Black Sea's cold intermediate layer in the middle of the western gyre, *Geophys. Res. Lett.*, *32*, L03604, doi:10.1029/2004GL021580.

Greinert, J., Y. Artemov, V. Egorov, M. De Batist, and D. McGinnis (2006), 1300-m-high rising bubbles from mud volcanoes at 2080 m in the Black Sea: Hydroacoustic characteristics and temporal variability, *Earth Planet. Sci. Lett.*, *244*(1–2), 1–15.

Gumerov, N. A., and G. L. Chahine (1998), Dynamics of bubbles in conditions of gas hydrate formation, paper presented at the 8th International Offshore and Polar Engineering Conference, *Int. Soc of Offshore and Polar Eng.*, Montreal, Canada.

Hayduk, W., and H. Laudie (1974), Prediction of diffusion-coefficients for nonelectrolytes in dilute aqueous-solutions, *AIChE J.*, *20*, 611–615.

Heeschen, K. U., A. M. Tréhu, R. W. Collier, E. Suess, and G. Rehder (2003), Distribution and height of methane bubble plumes on the Cascadia Margin characterized by acoustic imaging, *Geophys. Res. Lett.*, *30*(12), 1643, doi:10.1029/2003GL016974.

Hovland, M., and A. G. Judd (1988), *Seabed Pockmarks and Seepage: Impact on Geology, Biology and the Marine Environment*, 293 pp., Springer, New York.

Intergovernmental Panel on Climate Change (1996), *Climate Change 1995: The Science of Climate Change*, 572 pp., Cambridge Univ. Press, New York.

Jähne, B., K. O. Münnich, R. Bösinger, A. Dutzi, W. Huber, and P. Libner (1987), On the parameters influencing air-water gas exchange, *J. Geophys. Res.*, *92*, 1937–1949.

Jamialahmadi, M., C. Branch, and J. Müller-Steinhagen (1994), Terminal bubble rise velocity in liquids, *Trans. Inst. Chem. Eng.*, *72*, 119–122.

Johnson, A. I., F. Besik, and A. E. Hamielec (1969), Mass transfer from a single rising bubble, *Can. J. Chem. Eng.*, *47*, 559–564.

Joyce, J., and P. W. Jewell (2003), Physical controls on methane ebullition from reservoirs and lakes, *Environ. Eng. Geosci.*, *9*, 167–178.

Judd, A. G., M. Hovland, L. I. Dimitrov, G. García, and V. Jukes (2002), The geological methane budget at continental margins and its influence on climate change, *Geofluids*, *2*, 109–126.

King, M. B. (1969), *Phase Equilibrium in Mixtures*, 585 pp., Elsevier, New York.

Krastel, S., V. Spiess, M. Ivanov, W. Weinrebe, G. Bohrmann, P. Shashkin, and F. Heidersdorf (2003), Acoustic investigations of mud volcanoes in the Sorokin Trough, Black Sea, *Geo Mar. Lett.*, *23*, 230–238.

Lammers, S., and E. Suess (1994), An improved head-space analysis method for methane in seawater, *Mar. Chem.*, *47*, 115–125.

Leifer, I., and R. K. Patro (2002), The bubble mechanism for methane transport from the shallow sea bed to the surface: A review and sensitivity study, *Cont. Shelf Res.*, *22*, 2409–2428.

Lelieveld, J., P. J. Crutzen, and F. J. Dentener (1998), Changing concentration, lifetime and climate forcing of atmospheric methane, *Tellus, Ser. B*, *50*, 128–150.

Lewis, K., and B. Marshall (1996), Seep faunas and other indicators of methane rich dewatering on New Zealand convergent margins, *N. Z. J. Geol. Geophys.*, *39*, 181–200.

MacDonald, I. R., W. W. Sager, and M. B. Peccini (2003), Association of gas hydrate and chemosynthetic fauna in mounded bathymetry at mid-slope hydrocarbon seeps: Northern Gulf of Mexico, *Mar. Geol.*, *198*, 133–158.

MacDonald, I. R., L. C. Bender, M. Vardaro, B. Bernard, and J. M. Brooks (2005), Thermal and visual time-series at a seafloor gas hydrate deposit on the Gulf of Mexico slope, *Earth Planet. Sci. Lett.*, *233*, 45–59.

Maini, B. B., and P. R. Bishnoi (1981), Experimental investigation of hydrate formation behaviour of a natural gas bubble in a simulated deep sea environment, *Chem. Eng. Sci.*, *36*, 183–189.

Maneri, C. C. (1995), New look at wave analogy for prediction of bubble terminal velocities, *AIChE J.*, *41*, 481–487.

Marshall, D. R., S. Saito, and R. Kobayashi (1964), Hydrates at high pressures: part I. Methane-water, argon-water, and nitrogen-water systems, *AIChE J.*, *10*, 203–205.

McGinnis, D. F., and J. C. Little (2002), Predicting diffused-bubble oxygen transfer rate using the discrete-bubble model, *Water Res.*, *36*, 4627–4635.

McGinnis, D. F., A. Lorke, A. Wüest, A. Stöckli, and J. C. Little (2004), Interaction between a bubble plume and the near field in a stratified lake, *Water Resour. Res.*, *40*, W10206, doi:10.1029/2004WR003038.

McGinnis, D. F., S. Bocaniov, C. Teodoru, G. Friedl, A. Lorke, and A. Wüest (2006), Silica retention in the Iron Gate I reservoir on the Danube River: The role of side bays as nutrient sinks, *River Res. Appl.*, *22*, 441–456, doi:10.1002/rra.916.

Merewether, R., M. S. Olsson, and P. Lonsdale (1985), Acoustically detected hydrocarbon plumes rising from 2-km depths in Guaymas Basin, Gulf of California, *J. Geophys. Res.*, *90*, 3075–3085.

Michaelis, W., et al. (2002), Microbial reefs in the Black Sea fueled by anaerobic oxidation of methane, *Science*, *297*, 1013–1015.

Milkov, A. V. (2004), Global estimates of hydrate-bound gas in marine sediments: How much is really out there?, *Earth Sci. Rev.*, *66*, 183–197.

Naudts, L., J. Greinert, Y. Artemov, P. Staelens, J. Poort, P. Van Rensbergen, and M. De Batist (2006), Geological and morphological setting of 2778 methane seeps in the Dnepr paleo-delta, northwestern Black Sea, *Mar. Geol.*, *227*, 177–199.

Ostrovsky, I. (2003), Methane bubbles in Lake Kinneret: Quantification and temporal and spatial heterogeneity, *Limnol. Oceanogr.*, *48*, 1030–1036.

Paull, C. K., W. U. Ill, W. S. Borowski, and F. N. Spiess (1995), Methane-rich plumes on the Carolina continent rise associated with gas hydrates, *Geology*, *23*, 89–92.

Pecher, I. A., N. Kukowski, C. Huebscher, J. Greinert, J. Bialas, and G. W. Group (2001), The link between bottom-simulating reflections and methane flux into the gas hydrate stability zone—New evidence from Lima Basin, Peru Margin, *Earth Planet. Sci. Lett.*, *185*, 343–354.

Peng, D., and D. B. Robinson (1976), A new two-constant equation of state, *Ind. Eng. Chem. Fundam*, *15*, 59–64.

Reeburgh, W. S. (1996), "Soft spots" in the global methane budget, in *Microbial Growth on C1 Compounds*, edited by M. E. Lidstrom and F. R. Tabita, pp. 334–342, Springer, New York.

Rehder, G., R. S. Keir, E. Suess, and M. Rhein (1999), Methane in the northern Atlantic controlled by oxidation and atmospheric history, *Geophys. Res. Lett.*, *26*, 587–590.

Rehder, G., P. W. Brewer, E. T. Peltzer, and G. Friederich (2002), Enhanced lifetime of methane bubble streams within the deep ocean, *Geophys. Res. Lett.*, *29*(15), 1731, doi:10.1029/2001GL013966.

Rehder, G., I. Leifer, P. G. Brewer, G. Friederich, and E. T. Peltzer (2005), Physicochemical and hydrodynamical controls on methane bubble dissolution within the hydrate stability field, *Geophys. Res. Abstr.*, *7*, 06512.

Rettich, T. R., Y. P. Handa, R. Battino, and E. Wilhelm (1981), Solubility of gases and liquids. 13. High-precision determination of Henry's constants for methane and ethane in liquid water at 275 to 328 K, *J. Phys. Chem.*, *85*, 3230–3237.

Schmale, O., J. Greinert, and G. Rehder (2005), Methane emission from high-intensity marine gas seeps in the Black Sea into the atmosphere, *Geophys. Res. Lett.*, *32*, L07609, doi:10.1029/2004GL021138.

Schmid, M., K. Tietze, M. Halbwachs, A. Lorke, D. McGinnis, and A. Wüest (2003), How hazardous is the gas accumulation in Lake Kivu? Arguments for a risk assessment in light of the Nyiragongo Volcano eruption in 2002, *Acta Vulcanol.*, *15*, 115–122.

Simrad (1992), *Simrad EK500 Scientific Echo Sounder Instruction Manual*, Simrad Subsea P2170, Horten, Norway.

Singleton, V. L., P. Gantzer, and J. C. Little (2006), Linear bubble plume model for hypolimnetic oxygenation: Full-scale validation and sensitivity analysis, *Water Resour. Res.*, doi:10.1029/2005WR004836, in press.

Sloan, E. D. (1998), *Clathrate Hydrates of Natural Gases*, 641 pp., CRC Press, Boca Raton, Fla.

Stanev, E., J. Staneva, J. L. Bullister, and J. W. Murray (2004), Ventilation of the Black Sea pycnocline: Parameterization of convection, numerical simulations and validations against observed chlorofluorocarbon data, *Deep Sea Res., Part I*, *51*, 2137–2169.

St. Louis, V. L., C. A. Kelly, E. Duchemin, J. W. M. Rudd, and D. M. Rosenberg (2000), Reservoir surfaces as sources of greenhouse gases to the atmosphere: A global estimate, *BioScience*, *50*, 766–774.

Suess, E., M. E. Torres, G. Bohrmann, R. W. Collier, J. Greinert, P. Linke, G. Rehder, A. Trehu, K. Wallmann, G. Winckler, and E. Zuleger (1999), Gas hydrate destabilization: Enhanced dewatering, benthic material turnover and large methane plumes at the Cascadia convergent margin, *Earth Planet. Sci. Lett.*, *170*, 1–15.

Suess, E., et al. (2001), Sea floor methane hydrates at Hydrate Ridge, Cascadia Margin, in *Natural Gas Hydrates: Occurrence, Distribution, and Detection*, *Geophys. Monogr. Ser.*, vol. 124, edited by C. K. Paull, pp. 87–98, AGU, Washington, D. C.

Topham, D. R. (1984a), The formation of gas hydrates on bubbles of hydrocarbon gases rising in seawater, *Chem. Eng. Sci.*, *39*, 821–828.

Topham, D. R. (1984b), The modelling of hydrocarbon bubble plumes to include gas hydrate formation, *Chem. Eng. Sci.*, *39*, 1613–1622.

Torres, M. E., J. McManus, D. E. Hammond, A. de Angelis, K. U. Heeschen, S. L. Colbert, M. D. Tryon, K. M. Brown, and E. Suess (2002), Fluid and chemical fluxes in and out of sediments hosting methane hydrate deposits on Hydrate Ridge, OR, I: Hydrological provinces, *Earth Planet. Sci. Lett.*, *201*, 525–540.

Trehu, A. M., M. E. Torres, G. F. Moore, E. Suess, and G. Bohrmann (1999), Temporal and spatial evolution of gas hydrate-bearing accretionary ridge on the Oregon continental margin, *Geology*, *27*, 939–942.

Tryon, M. D., K. M. Brown, and M. E. Torres (2002), Fluid and chemical flux in and out of sediments hosting methane hydrate deposits on Hydrate Ridge, OR, II: Hydrological processes, *Earth Planet. Sci. Lett.*, *201*, 541–557.

Van Rensbergen, P., M. De Batist, J. Klerkx, R. Hus, J. Poort, M. Vanneste, N. Granin, O. Khlystov, and P. Krinitsky (2002), Sublacustrine mud volcanoes and methane seeps caused by dissociation of gas hydrates in Lake Baikal, *Geology*, *30*, 631–634.

Vasconcelos, J. M. T., S. P. Orvalho, and S. S. Alves (2002), Gas-liquid mass transfer to single bubbles: Effect of surface contamination, *AIChE J.*, *48*, 1145–1154.

Vasconcelos, J. M. T., J. M. L. Rodrigues, S. C. P. Orvalho, S. S. Alves, R. L. Mendes, and A. Reis (2003), Effect of contaminants on mass transfer coefficients in bubble column and airlift contactors, *Chem. Eng. Sci.*, *58*, 1431–1440.

Weiss, R. F. (1970), The solubility of nitrogen, oxygen and argon in water and seawater, *Deep Sea Res.*, *17*, 721–735.

Weiss, R. F. (1974), Carbon dioxide in water and seawater: The solubility of a non-ideal gas, *Mar. Chem.*, *2*, 203–215.

Whiticar, M. J. (2000), Can stable isotopes and global budgets be used to constrain atmospheric methane budgets?, in *Atmospheric Methane: Its*

Role in the Global Environment, edited by M. A. K. Khalil, pp. 63–85, Springer, New York.

Wilhelm, E., R. Battino, and R. J. Wilcock (1977), Low-pressure solubility of gases in liquid water, *Chem. Rev.*, *77*, 219–262.

Wüest, A., N. H. Brooks, and D. M. Imboden (1992), Bubble plume modeling for lake restoration, *Water Resour. Res.*, *28*, 3235–3250.

Zhang, Y.-X. (2003), Methane escape from gas hydrate systems in marine environment, and methane-driven oceanic eruptions, *Geophys. Res. Lett.*, *30*(7), 1398, doi:10.1029/2002GL016658.

Zheng, L., and P. D. Yapa (2000), Buoyant velocity of spherical and non-spherical bubbles/droplets, *J. Hydraul. Eng.*, *126*, 852–854.

Zheng, L., and P. D. Yapa (2002), Modeling gas dissolution in deepwater oil/gas spills, *J. Mar. Syst.*, *31*, 299–309.

Zimmermann, S., R. G. Hughes, and H. J. Flügel (1997), The effect of methane seepage on the spatial distribution of oxygen and dissolved sulphide within a muddy sediment, *Mar. Geol.*, *137*, 149–157.

Y. Artemov, Institute of Biology of the Southern Seas, Nakhimov Prospect, 99003 Sevastopol, Ukraine.

S. E. Beaubien, Department of Earth Sciences, University "La Sapienza," Piazzale Aldo Moro, 5, Roma I-00185, Italy.

J. Greinert, Marine Geosystems, Leibniz-Institut für Meereswissenschaften IFM-GEOMAR, Wischhofstrasse 1-3, D-24148 Kiel, Germany.

D. F. McGinnis and A. Wüest, Surface Waters–Research and Management, Swiss Federal Institute of Aquatic Science and Technology, Eawag, CH-6047 Kastanienbaum, Switzerland. (dan.mcginnis@eawag.ch)